

Can phantom transition at $z \sim 1$ restore the Cosmic concordance?

Zhihuan Zhou,^{1*} Gang Liu, Yuhao Mu, Lixin Xu[†]

Institute of Theoretical Physics, School of Physics, Dalian University of Technology, Dalian, 116024, China

Accepted 2022 January 4. Received 2021 December 21; in original form 2021 October 21

ABSTRACT

The tension among inferences of Hubble constant (H_0) is found in a large array of datasets combinations. Modification to the late expansion history is the most direct solution to this discrepancy. In this work, we examine the viability of restoring the cosmological concordance with a novel version of transitional dark energy (TDE). The main anchors for the cosmic distance scale: cosmic microwave background (CMB) radiation, baryon acoustic oscillation (BAO), and Type Ia supernova (SNe Ia) calibrated by Cepheids form a “impossible trinity”, i.e., it’s plausible to reconcile with any two of the three but unlikely to accommodate them all. Particularly, the tension between BAO and the calibrated SNe Ia can not be reconciled within the scenarios of late dark energy. Nevertheless, our analysis suggests that the TDE model can reconcile with CMB and SNe Ia calibrated by its absolute magnitude (M_B), when the equation of state (EoS) of DE transits around $z \sim 1$. Meanwhile, we see a positive sign that the EoS transits with the inclusion of a local prior on M_B , whereas the opposite is true without the M_B prior.

Key words: Dark energy – Cosmology

1 INTRODUCTION

The precise determination of the Hubble constant H_0 , which requires both accurate astrophysical and cosmological modeling, is crucial for modern cosmology. Historically, H_0 is measured directly via the classical distance ladder (Sandage et al. (2006)) in the local universe, while in the early universe, H_0 is extracted indirectly from angular size of the sound horizon r_s and the shapes of the acoustic peaks in the cosmic microwave background (CMB) radiation (Hinshaw et al. (2013); Ade et al. (2014)). These measurements disagree at $4 \sim 6\sigma$ significance, e.g., $H_0 = 73.2 \pm 1.3$ from SH0ES collaboration (Riess et al. (2021)) and $H_0 = 67.4 \pm 0.5$ from Planck 2018 data¹ (Aghanim et al. (2018)). Several independent H_0 probes of the late-universe have reached competitive accuracy with the distance ladder, such as measurements of the strongly lensed quasar systems (Wong et al. (2020)), obtaining $H_0 = 73.3^{+1.7}_{-1.8}$. Since the H_0 tension between late and early universe is found in a large array of differing datasets combinations (see Verde et al. (2019); Perivolaropoulos & Skara (2021a) for a recent review), it’s unnatural to attribute the disagreement solely to systematic errors². Hence, this tension may be a sign of physics beyond the standard Λ CDM cosmology.

There exist varied theoretical proposals to explain or ameliorate the

H_0 discrepancy, ranging from new physics in early-time ($z \gtrsim 1100$, pre-recombination) to late-time ($z \lesssim 2$) universe (see Di Valentino et al. (2021) for a review). Within the framework of General Relativity (GR), it is natural to consider the dynamical DE, i.e., replacing cosmological constant Λ with a scalar field (Barboza & Alcaniz (2008); Armendariz-Picon et al. (2000); Linder (2003); Jassal et al. (2005); Armendariz-Picon et al. (2001); Caldwell (2002); Guo et al. (2005); D’Amico et al. (2021)) or a DE equation of state (EoS) parameterization (see Li et al. (2011) for a review). Whereas, it is proved the converse that Quintessence (a minimally coupled scalar) always makes Hubble tension worse than Λ (Banerjee et al. (2021)). Other tentative solutions include interacting DE (Kumar & Nunes (2016); Yang et al. (2018); Pan et al. (2020); Di Valentino et al. (2020); Nunes & Di Valentino (2021)), modified gravity (Saridakis et al. (2021); Nunes (2018); Raveri (2020); Yan et al. (2020); Frusciante et al. (2020); D’Agostino & Nunes (2020); Ballardini et al. (2020)) as well as other possibilities (Hart & Chluba (2018); Chiang & Slosar (2018); Yang et al. (2019); Jedamzik & Pogosian (2020); Sekiguchi & Takahashi (2020); Vagnozzi (2020)). Recently, the binned analysis of H_0 is employed in (Wong et al. (2020); Dainotti et al. (2021)) to investigate a possible evolutionary trend for H_0 .

These proposals must also stand up to the scrutiny of current Large-Scale Structure (LSS) surveys (Abbott et al. (2018); Alam et al. (2017); Hildebrandt et al. (2020); Hikage et al. (2019)), which have delivered precise cosmological constraints. Interestingly, the inference of H_0 value in both CMB and LSS surveys depend on the precise determination of sound horizon r_s , thus, a reduction of the sound horizon by increasing the expansion rate just prior to recombination (with additional energy density components, e.g., exotic early dark energy (EDE) (Poulin et al. (2019); Gogoi et al. (2020)), acoustic dark energy (ADE) (Lin et al. (2020)) seems to be the “least unlikely to be successful” (Knox & Millea (2020)) approach to solve the H_0 tension. However, the addition of EDE

* E-mail: 11702005@mail.dlut.edu.cn

† E-mail: lxxu@dlut.edu.cn

¹ The obtained H_0 by alternative methods varies between these measurements. One example is the recent measurement $H_0 = 69.8 \pm 2.2$ from tip of the red giant branch (TRGB) calibration (Freedman (2021)).

² Extensive works have focused on whether this discrepancy can be caused by yet unknown systematic effects. Recent work in Mortsell et al. (2021) suggest that, by choosing different Cepheid colorluminosity calibration method, the obtained H_0 could be much more compatible with the Planck value. To show the application of the late dark energy to the H_0 fit, we will focus on the SH0ES result that has the largest deviation from the Planck result.

or another component would suppress the growth of perturbations prior to recombination, which changes the amplitudes and phases of the CMB acoustic peaks in complex ways and would bring in new tension with the density fluctuation amplitude, σ_8 . Moreover, given a certain shift in r_s , the shift in H_0 needed in the CMB to match observations will be different from the one needed to match the LSS observations, introducing a currently non-existing tension (Hill et al. (2020)).

In the late-DE scenarios, the sound horizon at last scattering $r_s(z_*)$ is preserved from the modification of late expansion history. With the acoustic scale ($D_A(z_*)/r_s(z_*)$) fixed by CMB, an upward shift on H_0 is compensated by the increase of $D_A(z_*)$, which can be implemented by raising the “dilution rate” of DE density. This scenario can be realized by a wide class of “phantom-like” DE (Caldwell (2002); Caldwell et al. (2003); Guo et al. (2005); Alestas et al. (2020)). Although the phantom transition of DE at late time is able to provide an apparent resolution of the H_0 tension, the underlying tension of the SNIa absolute magnitude (M_B) have not been taken into account. Recent works in Camarena & Marra (2021); Benevento et al. (2020); Alestas et al. (2021b) have studied phantom transition at very-low redshift ($z < 0.1$) accompanied by an M_B transition or a rapid transition of the effective gravitational constant (G_{eff}) at $z < 0.01$ (Marra & Perivolaropoulos (2021)), in order to address both the H_0 tension and M_B tension. Being backed up by several observational hints (Alestas et al. (2021a); Perivolaropoulos & Skara (2021b)), this double transition model proves to be successful in addressing the S_8 tension as well (Marra & Perivolaropoulos (2021)). In the recently proposed phenomenological emergent dark energy model (PEDE) (Li & Shafieloo (2019)) model and its generalized version (Li & Shafieloo (2020); Hernández-Almada et al. (2020)), the DE is negligible at early times but dominates at late-time, providing an alternative solution to the coincidence problem (Hernández-Almada et al. (2020)). If only the local H_0 measurements and CMB data are taken into consideration, this scenario seems ideal to solve the H_0 tension because the imprints of late-universe modification on the CMB spectra can be counteracted by a shift in H_0 . However, the numerical analysis in (Rezaei et al. (2020); Benaoum et al. (2020)) suggests that, the PEDE model is not well compatible with SN Ia and LSS surveys, especially the $f\sigma_8(z)$ data from RSD observations (Rezaei et al. (2020)). Such incompatibility is mainly caused by the sharp transition of EoS at present, hence one may consider altering the scale at which the EoS of DE transits to avoid the tension. Using Gaussian process regression, Keeley et al. (2019) suggests that when the EoS transits rapidly at $1 \lesssim z \lesssim 2$, the growth of the perturbation is slower than fiducial Λ CDM model for $z \lesssim 1$, while the study in Alestas & Perivolaropoulos (2021) suggest that deforming $H(z)$ with CPL parameterization worsens the growth tension. As a result of these concerns, we proposed a novel version of transitional dark energy (TDE) model (based on the research in Keeley et al. (2019); Bassett et al. (2002)), which is captured by the transitional scale a_c . In this scenario, the DE behaves like the cosmological constant Λ at late-time and goes through a rapid transition in the EoS at a_c .

The outline of this paper is as follows: in section 2 we take a brief review of the key observations associated with H_0 tension. In section 3, we briefly introduce the TDE model as well as its cosmological features. In section 4, we describe our numerical implementation of EDE model and the datasets used in our analysis. The numerical results of the Markov chain Monte Carlo (MCMC) analysis are presented in section 5. The discussion and conclusions are presented in section 6.

2 MATCHING THE CMB

Measurements of the CMB spectra precisely determine the angular acoustic scale θ_s (transverse direction) and the “shift parameter” R (line-of-sight direction), defined as (Chen et al. (2019))

$$\theta_s = r_s(z_*)/D_A(z_*), \quad R(z_*) \propto \omega_m^{\frac{1}{2}} D_A(z_*), \quad (1)$$

where z_* is the redshift at the photon decoupling epoch, $D_A(z) = \int_0^z \frac{dz'}{H(z')}$ is the angular diameter distance and r_s is the comoving sound horizon, defined by

$$r_s(z_*) = \int_{z_*}^{\infty} \frac{dz}{H(z)} c_s(z), \quad (2)$$

where $c_s(z)$ is the sound speed of the coupled photon-baryon fluid. In matter-radiation dominated era, an approximation of Hubble rate reads

$$H(z) \propto \left[\omega_r(1+z)^4 + \omega_m(1+z)^3 \right]^{\frac{1}{2}}, \quad (3)$$

which have no dependence on H_0 when $\omega_m \equiv \Omega_{m,0}h^2$ and $\omega_r \equiv \Omega_{r,0}h^2$ are fixed at given values (hereinbelow). Thus, a shift of the local expansion rate H_0 as well as modifications to the expansion history after last scattering ($z < z_*$) preserves the sound horizon $r_s(z_*)$.

Within the scenarios of late-DE, the DE component has no effective presence in the past, and thus have no impact on $r_s(z_*)$. Unlike EDE changes the power spectrum in a complex way (Poulin et al. (2018)), the presence of late-DE changes only the traveling distance of the free streaming photons in the late universe, resulting in a linear shift in power spectrum. Such a shift can be perfectly offset by adjustment of H_0 value, thus, the best-fit H_0 can be conveniently obtained by “shooting”³ the *Planck* best-fit $D_A(z_*)$ in Λ CDM model⁴. To verify the above argument, we calculate the disparity between the angular power spectrum calculated in Λ CDM model and in late-DE scenarios (C_ℓ^Λ), e.g., TDE, PEDE (Li & Shafieloo (2019)) calibrated by the best-fit H_0 . The results shown in Fig. 1 indicates that the differences is much smaller than the cosmic variance, i.e.,

$$\frac{2\ell+1}{2} \left(\frac{C_\ell^X - C_\ell^\Lambda}{C_\ell^\Lambda} \right)^2 < 0.01. \quad (4)$$

Consequently, the influence of late-DE on CMB is equivalent to a H_0 shift which preserves the overall shape of the power spectrum. On the other hand, for a given H_0 prior, the *Planck*- Λ CDM best-fit spectrum can always be matched by adjusting late-DE parameters, thus, the tension between SH0ES and CMB is resolved within late-DE scenarios. It should be noted that, in this work DE is treated as an effective fluid with equations of evolution for density perturbation δ_{fld} and velocity θ_{fld} , respectively, given in (Ballesteros & Lesgourgues (2010)). Solving these equations requires the specification of the fluid EoS $w(z)$ (see discussion in section 3), the effective sound speed of DE $c_s^2 \equiv \delta p / \delta \rho$ (evaluated in the fluid rest frame), and adiabatic sound speed $c_a^2 \equiv \dot{p} / \dot{\rho}$. We fix $c_s^2 = 1$ so that the fluid can not be clustered, and $c_a^2 = w - \dot{w}/3\mathcal{H}(1+w)$ with $\mathcal{H} \equiv aH$ the conformal Hubble rate.

With *Planck* the best-fit H_0 value, we can calculate other key

³ By “shooting”, we mean that when a default value of $D_A(z_*)$ is chosen, we adjust H_0 until a suitable value is found which gives the correct $D_A(z_*)$. This algorithm is frequently used in CLASS (Lesgourgues (2011)).

⁴ As is indicated in Eq. (1), the key features of the CMB spectrum (θ_s and $R(z_*)$) depend only on $D_A(z_*)$ when ω_m and r_s are preserved.

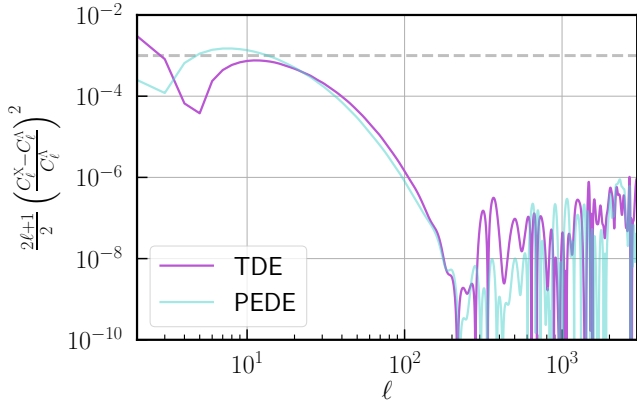


Figure 1. The disparity between the angular power spectrum calculated in TDE, PEDE (Li & Shafieloo (2019)) model (C_ℓ^X) and in Λ CDM model (C_ℓ^Λ) divided by the cosmic variance, i.e., $\frac{2\ell+1}{2} \left(\frac{C_\ell^X - C_\ell^\Lambda}{C_\ell^\Lambda} \right)^2$. Noting that H_0 is set to the best-fit value obtained by “shooting” (see section 2), while other parameters are set to the *Planck* best-fit values.

observables (S_8 , $f\sigma_8(z)$) to see whether the solution of H_0 tension is at the cost of bringing in new tensions with other observations. For example, in LSS surveys the angular acoustic scale θ_s could also be extracted from galaxy power spectrum at low-redshift ($z \approx z_{\text{LSS}} \sim 0.3$), denoting as:

$$\theta_{\text{LSS}} \approx \frac{r_s(z_*)}{(D_A(z_{\text{LSS}})^2 \cdot cz_{\text{LSS}}/H(z_{\text{LSS}}))^{\frac{1}{3}}}, \quad (5)$$

with approximation $r_s(z_*) \sim r_s(z_d)$, where z_d is redshift at drag epoch, and $D_H(z) \equiv 1/H(z)$. We show in Fig. 2 the “shooting” results of the WCDM model (negative cosmological constant) (Visinelli et al. (2019)) and TDE model, the details of the TDE model will be discussed in the next section).

3 MODEL

According to the recent surveys, the universe on large scale is almost flat and can be well described by Friedmann-Lemaitre-Robertson-Walker (FLRW) metric. The Hubble parameter within this framework can be expressed as:

$$H(z) = H_0 \left[\Omega_{m,0}(1+z)^3 + \Omega_{r,0}(1+z)^4 + \Omega_{\text{DE}} \right]^{\frac{1}{2}}, \quad (6)$$

where $\Omega_{m,0}$, $\Omega_{r,0}$ are the present time matter and radiation density, respectively. The dark energy density Ω_{DE} can be described as:

$$\Omega_{\text{DE}}(z) = \Omega_{\text{DE},0} \times \exp \left[3 \int_0^z \frac{1+w(z')}{1+z'} dz' \right], \quad (7)$$

where Ω_{DE} is ratio of DE density to the critical density ($\rho_{\text{DE}}/\rho_{\text{crit},0}$). The exponential part of Eq. 7 indicates that, a smaller value of w would translate into a faster dilution rate of DE. This effect suppresses the dilation of the late universe and is well compensated by an upward shift in H_0 , thus, the H_0 tension is relieved.

3.1 Transitional Dark Energy

We formulate a novel version of transitional dark energy (TDE) model (see (Keeley et al. (2019); Bassett et al. (2002); Shafieloo

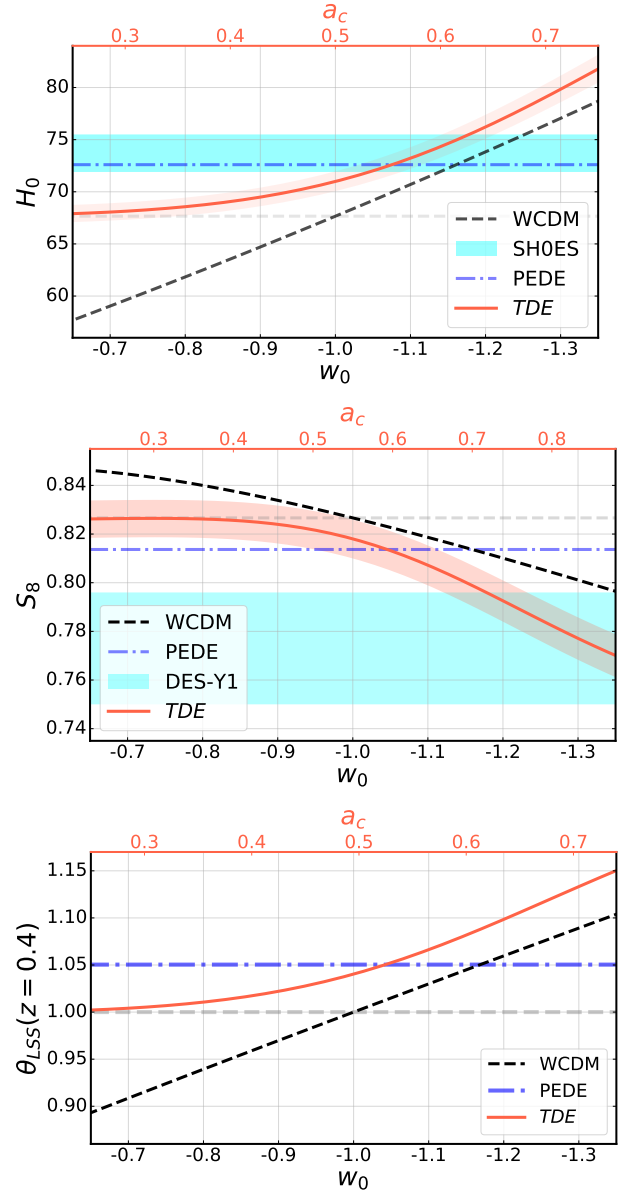


Figure 2. The *Planck* best-fit H_0 (top panel), S_8 (middle panel) and θ_{LSS} (bottom panel) for different late-DE models. Noting that the best-fit observable are obtained by “shooting” $D_A(z_*)$ (see section 2). The shaded regions correspond to the error propagation from 68% confidence levels of the *Planck* distance prior. The horizontal band correspond to the SH0ES constrains i.e $H_0 = 73.2 \pm 1.3$ (top panel) and DES-Y1 constrains i.e $S_8 = 0.773^{+0.026}_{-0.020}$ (middle panel).

et al. (2009)) for discussions of similar models), with the EoS of DE written as:

$$w(z) = w_0 - \frac{1}{2} \left[\tanh \left(3 \left(\frac{1}{a} - \frac{1}{a_c} \right) \right) + 1 \right]. \quad (8)$$

To recover Λ CDM model when $a \gtrsim a_c$, we fix $w_0 = -1$ (denote as TDE(1p)). In such case we have the EoS of DE evolving from $w = -2$ at high redshift to $w = -1$ at low redshift, which recovers the case in Covariant Galileon cosmology under the right initial conditions (De Felice & Tsujikawa (2010)). As is illustrated in Fig. 3 the EoS of DE remains constant at late-time then endures a rapid transition at the critical scale a_c . With the increase of a_c , the inferred value

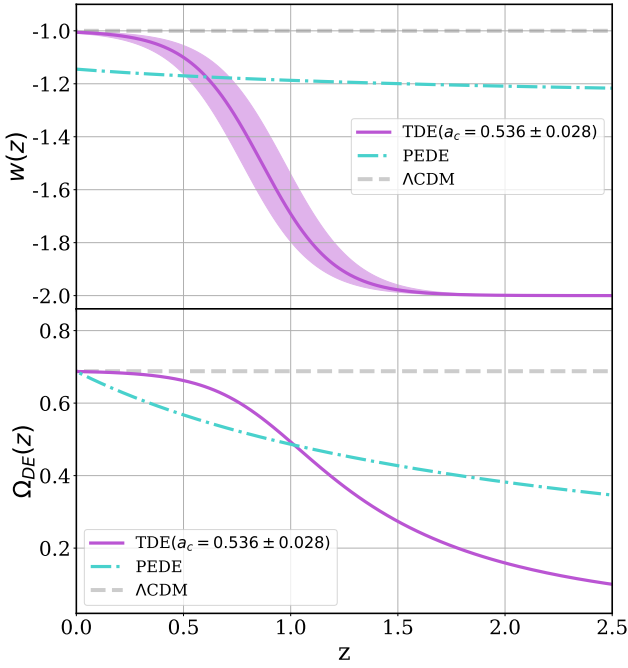


Figure 3. The evolution of EoS of DE (upper panel) and density ratio $\Omega_{DE} \equiv \rho_{DE}/\rho_{crit,0}$ (lower panel) for different DE models, respectively. The parameters are set in terms of the best-fit values of the joint *Planck*+ M_B +SNe datasets, e.g., $a_c = 0.536 \pm 0.028$ (see Table 2). The shaded bands correspond to the 68% confidence levels, while the gray dashed line corresponds to the Λ CDM model as a references.

of H_0 increases, while the shifts on S_8 is the reverse. However, our analysis suggests that the transition of DE could not relieve the $f\sigma_8$ tension (see Fig. 4). Owing to the fact that, the growth function $f(z)$ is boosted at $a \lesssim a_c$, thus the solution of H_0 and S_8 tension (raising a_c) is at the cost of exacerbating $f\sigma_8$ tension.

Due to the resemblance to Λ CDM model at late universe, TDE(1p) could largely avoid the mismatch with SNe datasets at the same time fit with the acoustic scale determined by CMB. However, this scenario does not relieve the mismatch between the local distance ladder and BAO surveys, both of which can be directly related to the supernova absolute magnitude M_B . With the calibration of the sound horizon $r_s(z_d)$ (determined by CMB), the BAO experiments (Alam et al. 2017) anchor the distance scales ($D_A(z \sim 0.3)$) at the late-universe. Using the parametric-free inverse distance ladder (Camarena & Marra 2020b) these scales can be propagated to SNIa absolute magnitude:

$$M_B^{P18} = -19.401 \pm 0.027 \text{ mag}, \quad (9)$$

which disagrees with the M_B prior obtained from SH0ES (Riess et al. 2021) by demarginalization method at 3.4σ (Camarena & Marra 2020a). Note that $r_s(z_d)$ is preserved within the scenario of late-DE. In this light, to address the above discussed M_B tension, one may consider a rapid phantom transition of the EoS of DE at $z < 0.1$ accompanied by a similar transition in the value of M_B (Alesta et al. 2021b; Marra & Perivolaropoulos 2021).

4 STATISTICAL METHODOLOGY AND DATASETS

We implement TDE scenario as modifications to the publicly available Einstein-Boltzmann code CLASS (Lesgourgues (2011); Blas

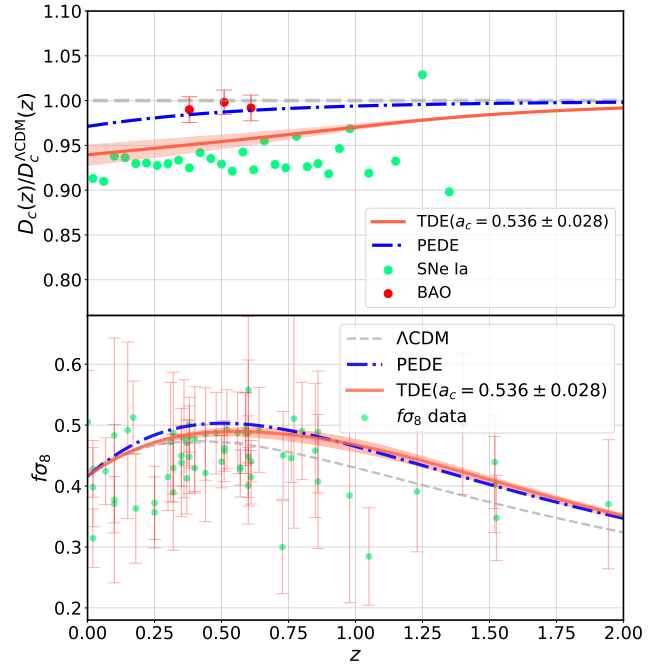


Figure 4. The relative comoving distances ($D_c(z)/D_c^{\Lambda\text{CDM}}(z)$) are shown in the top panel, and $f(z)\sigma_8(z)$ are shown in the bottom panel, respectively. The cosmological parameters are set to the best-fit values of joint *Planck*+ M_B +SNe datasets. The SNe constrain only the ratio of the distances D_L/D_{H_0} , so the absolute scale of the SNe data points in the top panel is calibrated by the M_B^{R20} prior (Efstathiou (2021)), i.e., $M_B = -19.244 \pm 0.037$. The BAO measurements constrain $D_c \times (r_{d,\text{fid}}/r_d)$, and thus the BAO data point are corrected with the factor $r_d/r_{d,\text{fid}}$ ($r_{d,\text{fid}} = 147.78$). Noting that, the inferred values of r_d are the same for PEDE (Li & Shafieloo (2019)) and TDE model (when ω_m and ω_r are fixed). The 63 observational $f\sigma_{8,obs}(z)$ RSD data points are collected by (Kazantzidis & Perivolaropoulos (2018)), which have been corrected by the AP factor (Li et al. (2021)) calculated based on TDE model.

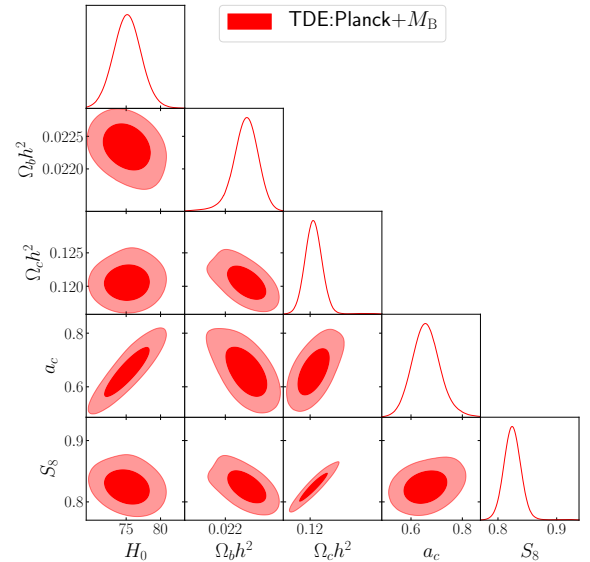


Figure 5. Cosmological parameter constraints from the combination of *Planck* 2018 distance prior and the M_B^{R20} prior; the contours show 1 σ and 2 σ posteriors for the TDE model.

Parameter	Prior
H_0	[50, 90]
$\Omega_b h^2$	[0.01, 0.1]
$\Omega_c h^2$	[0.05, 0.3]
$a_c(\text{TDE})$	[0.01, 1.0]

Table 1. Flat priors assumed on the cosmological parameters associated with the TDE model and Λ CDM model

et al. (2011)) package. The non-linear matter power spectrum required by redshift-space distortion (RSD) likelihoods are computed using the “HMcode” (Mead et al. (2015); Mead (2017); Mead et al. (2020)) implemented in CLASS. The MCMC analyses are performed using the publicly available code *Cobaya* (Torrado & Lewis (2020)) package with a Gelman-Rubin (Gelman & Rubin (1992)) convergence criterion $R - 1 < 0.05$. The plots have been obtained using the *GetDist* (Lewis (2019)) package.

The following datasets are considered in the MCMC analyses:

4.1 CMB

We consider the CMB distance prior from final *Planck* 2018 release. Noted that, in late-DE scenarios, the shape of the power spectrum (with the same matter and radiation density) is identical to that of Λ CDM cosmology at $\ell \gtrsim 10$ (for small ℓ s the covariance is largely dominated by cosmic variance). In this case, the fit of the distance prior is equivalent to that of the angular power spectrum, while this is not true for EDE scenarios. The analysis with the *Planck* 2018 low- ℓ TT+EE and *Planck* 2018 high- ℓ TT+TE+EE temperature and polarization power spectrum (Aghanim et al. (2020)) are shown in Appendix C

4.2 Hubble Constant

The most recent SH0ES measurement indicates that $H_0 = 73.2 \pm 1.3$ (Riess et al. (2021)), which shows a tension at 4.4σ with the *Planck* (Aghanim et al. (2018)) value of H_0 assuming a minimal Λ CDM model. Note that the determination of H_0 by the SH0ES collaboration have fixed the deceleration parameter to the standard Λ CDM model value of $q_0 = -0.55$. To avoid inconsistency and double counting of the low- z SNe samples (Efsthathiou (2021)), we adopt a prior on the SNe Ia absolute magnitude

$$M_B^{\text{R20}} = -19.244 \pm 0.037 \text{ mag} \quad (10)$$

which is derive using the demarginalization methodology of Camarena & Marra (2020a). With an uninformative flat prior for q_0 , the above M_B prior gives $H_0 = 75.35 \pm 1.68$. We denote as σ_{SH0ES} the effective number of σ 's that the Hubble measurement is away from this value. See Camarena & Marra (2021) for a detailed discussion of the local M_B likelihoods.

4.3 Supernovae Type Ia

The 1048 Supernovae Type Ia data points distributed in redshift interval $z \in [0.01, 2.3]$, known as the Pantheon sample (Scolnic et al. (2018)), which provide accurate relative luminosity distances. We utilize the likelihood as implemented in *Cobaya*.

4.4 LSS

The LSS dataset which probes the low-redshift universe are considered, which include:

- BAO: measurements of the BAO signal with their full covariance matrix from BOSS DR12 (Alam et al. (2017)). Radial and transverse BAO measurements from Ly α Forests SDSS DR12 (Bautista et al. (2017)). Angle averaged BAO measurement from 6DF Galaxy (Beutler et al. (2011)), from quasar sample from BOSS DR14 (Gil-Marín et al. (2018)).

- RSD: SDSS BOSS DR12 (Alam et al. (2017)) measurements of $f\sigma_8(z)$, at $z = 0.38, 0.51$ and 0.61 . We include the full covariance of the joint BOSS DR12 BAO and RSD data (denote as FS). Noting that the measured $f\sigma_8(z)$ at different redshifts is not fully independent. Also, the $f\sigma_8(z)$ data is correlated with the BAO signal, thus, it's hard obtain the full covariance of the datasets compiled from different surveys. In view of this, the compilation of 63 $f\sigma_{8,\text{obs}}(z)$ RSD data points (Kazantzidis & Perivolaropoulos (2018)) are not included in the MCMC analysis, but only displayed as an illustration of the $f\sigma_8$ tension.

- DES: shear-shear, galaxy-galaxy, and galaxy-shear two-point correlation functions (“3x2pt”), measured from 26 million source galaxies in four redshift bins and 650,000 luminous red lens galaxies in five redshift bins, for the shear and galaxy correlation functions, respectively. We utilize a Gaussian prior on S_8 derived by the DES-Y1 likelihood as is suggested in (Hill et al. (2020)).

It's worth noting that TDE are extended from Λ CDM model, and thus share with Λ CDM model the six parameters. We fix three of the six parameter ($n_s, A_s, \tau_{\text{reio}}$) associated with the overall shape of the CMB spectrum to the best-fit value given by *Planck* 2018 (Aghanim et al. (2018)). Next, we consider as baseline a 4-dimensional parameter space described by the following parameters: the Hubble constant H_0 , the baryon energy density $\Omega_b h^2$, cold dark matter energy density $\Omega_c h^2$, and the transitional scale a_c for TDE. We assume flat uniform priors on all these parameters, as are shown in Table 1.

5 RESULTS AND DISCUSSION

For the cosmological analysis, we fit the TDE model to different combinations of the above discussed datasets. As a comparison, we also include the analysis of the Λ CDM model. In order to compare among these models, we compute the Bayesian evidence ε , which is a crucial quantity for model selection and has been widely used in cosmology (Mehrabadi & Basilakos (2018); Rezaei et al. (2020); Lonappan et al. (2018); Saini et al. (2004)). Further, given two models M_i and M_j one can use the Jeffreys' scale (Jeffreys (1961)) to measure the significant difference between two models, i.e., $\Delta \ln \varepsilon = \ln \varepsilon_{M_i} - \ln \varepsilon_{M_j}$. The model pair difference provides the following situations:

- $0 < \Delta \ln \varepsilon < 1.1$ suggests weak evidence against M_j model when compared with M_i .
- for $1.1 < \Delta \ln \varepsilon < 3$ there is a definite evidence against model M_2 .
- for $3 < \Delta \ln \varepsilon$ there is a strong evidence against model M_2 .

Correspondingly, the evidence is against M_i model when $\Delta \ln \varepsilon < 0$. In addition to the evidence, we also include the computation of the Akaike Information (AIC) (Akaike (1974)), given by:

$$\text{AIC} = \chi_{\text{min}}^2 + 2k \quad (11)$$

where k is the number of fitting parameters. For brevity, we denote

Model	Dataset	H_0	S_8	a_c	σ_{SH0ES}	χ^2_{min}	$\Delta\chi^2$	$\ln \varepsilon$	$\Delta \ln \varepsilon$
TDE	<i>Planck</i>	77.0 ± 8.0	$0.815^{+0.032}_{-0.027}$	> 0.562	0.2	2.9	0.0	-8.73	0.69
	<i>Planck</i> + M_B	75.2 ± 1.7	0.825 ± 0.014	0.658 ± 0.049	0.1	4.6	-23.5	-11.54	-9.10
	PMS (<i>Planck</i> + M_B + SNe)	71.59 ± 0.81	0.825 ± 0.011	0.548 ± 0.029	2.0	1045.0	-17.5	-533.03	-5.10
	PMS + S_8	71.77 ± 0.90	0.812 ± 0.012	$0.531^{+0.045}_{-0.040}$	1.9	1051.3	-14.7	-535.07	-4.06
	PMS + S_8 + BAO	$69.55^{+0.73}_{-0.94}$	0.816 ± 0.015	0.420 ± 0.082	3.0	1062.3	-5.6	-540.25	-0.89
	PMS + S_8 + BAO + FS	69.16 ± 0.76	0.814 ± 0.012	$0.375^{+0.12}_{-0.043}$	3.2	1068.2	-3.5	-543.41	0.15
		H_0	S_8	–	σ_{SH0ES}	χ^2_{min}	$\Delta\chi^2$	$\ln \varepsilon$	$\Delta \ln \varepsilon$
LCDM	<i>Planck</i>	66.77 ± 0.54	0.836 ± 0.013	–	4.9	2.9	–	-8.04	–
	<i>Planck</i> + M_B	$67.41^{+0.46}_{-0.65}$	$0.820^{+0.015}_{-0.011}$	–	4.5	28.1	–	-20.64	–
	PMS	67.74 ± 0.50	0.813 ± 0.012	–	4.3	1062.5	–	-538.13	–
	PMS + S_8	$68.34^{+0.76}_{-0.33}$	$0.798^{+0.014}_{-0.020}$	–	4.0	1066.0	–	-539.13	–
	PMS + S_8 + BAO	$68.26^{+0.59}_{-0.38}$	$0.800^{+0.013}_{-0.015}$	–	4.0	1067.9	–	-541.14	–
	PMS + S_8 + BAO + FS	68.35 ± 0.31	0.800 ± 0.010	–	4.1	1071.7	–	-543.26	–

Table 2. The mean and $1-\sigma$ constraints on H_0 and S_8 in the TDE model (top panel) and Λ CDM model (bottom panel), as well as the constraints on a_c for TDE model. We have also shown in the third to the last column the effective number of σ 's that the Hubble measurement is away from SH0ES. The χ^2 statistics are shown in the last two columns, where $\Delta\chi^2$ is the inferred χ^2_{min} compared with Λ CDM model. In the last column, $\Delta \ln \varepsilon$ denotes difference of Bayesian evidence between Λ CDM model and the TDE model, i.e., $\Delta \ln \varepsilon = \ln \varepsilon_{\Lambda\text{CDM}} - \ln \varepsilon_{\text{TDE}}$.

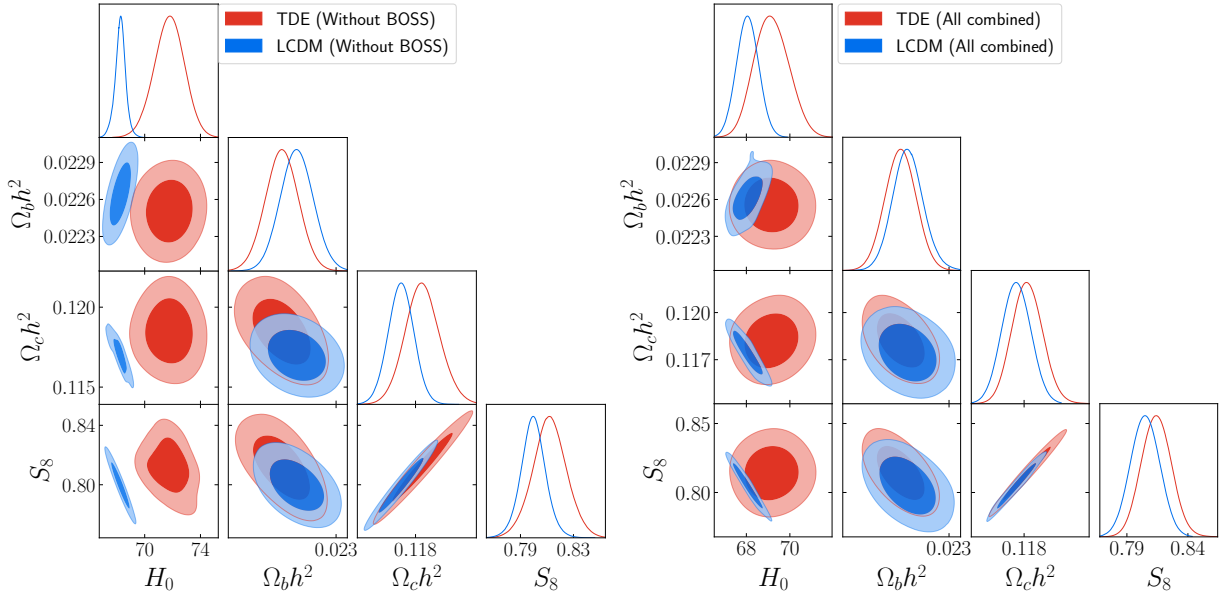


Figure 6. The right panels show the cosmological parameters constraints from the combination of *Planck* 2018 distance prior; BAO data from 6dF, SDSS DR14, and BOSS DR12; Pantheon SNIa data; the M_B^{R20} prior; BOSS DR12 RSD data; and the S_8 prior derived from DES-Y1 3x2pt data. The red (blue) contours show 1σ and 2σ posteriors for the TDE(Λ CDM) model. In the left panel, we show 1σ and 2σ posteriors for the TDE(Λ CDM) model by constraints from the above combination of without the full covariance of the joint BOSS DR12 BAO and RSD data (denote as without BOSS); The posteriors for all datasets combinations are shown in the right panel as a contrast (denote as all combined).

the combination of likelihoods without LSS data as PMS (*Planck* + M_B + SNe). In Table 2 we report the constraints at 68% CL on the H_0 and some key derived quantities for several datasets combinations considered in this work. Detailed constraints on cosmological parameters and χ^2 statistics can be found in Tables 3–5. The triangular

plot with the 1D posterior distributions and the 2D contour plots for these parameters are shown in Fig. 5–7.

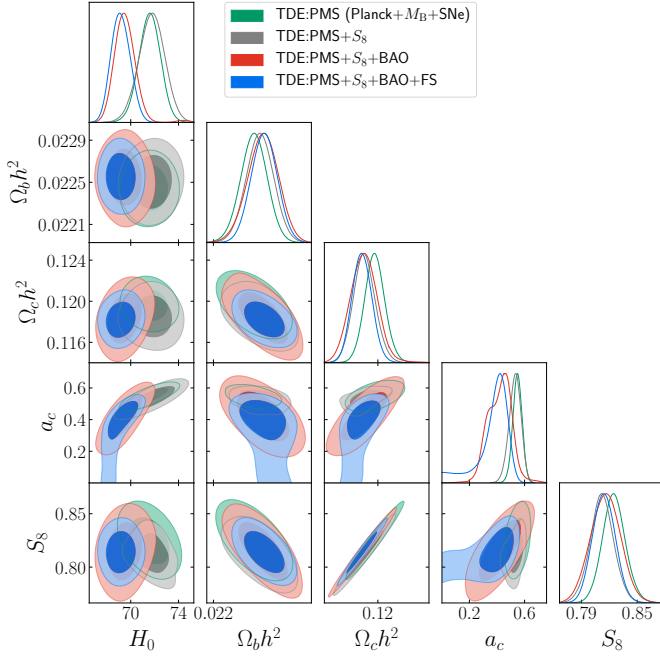


Figure 7. Constraints on TDE scenario from various dataset combinations. The contours show 1σ and 2σ posteriors. The green contours show results for the combination *Planck* distance prior, SNIa and M_B prior; the dark contours additionally include a prior on S_8 ; and the red contours further include BAO data; the blue contours add the RSD data (constraints on $f\sigma_8$). Noting that, the inclusion of a prior on S_8 slightly alleviate the tension with SH0ES and shift a_c toward 1.

Dataset	<i>Planck</i> + M_B	
Model	TDE	Λ CDM
H_0	75.2 ± 1.7	$67.41^{+0.46}_{-0.65}$
$\Omega_b h^2$	$0.02233^{+0.00016}_{-0.00015}$	$0.02248^{+0.00012}_{-0.00017}$
$\Omega_c h^2$	$0.1206^{+0.0011}_{-0.0013}$	$0.1186^{+0.0012}_{-0.0011}$
a_c	0.658 ± 0.049	–
S_8	$0.825^{+0.013}_{-0.015}$	$0.820^{+0.015}_{-0.011}$
$\chi^2_{M_B}$	0.8 ± 1.2	24 ± 4
χ^2_{Planck}	3.9 ± 6.4	4.2 ± 3.4
χ^2_{tot}	4.6 ± 6.6	28.1 ± 1.9
$\Delta\chi^2$	–23.5	–
ΔAIC	–21.5	–
$\Delta \ln \varepsilon$	–9.10	–

Table 3. The mean $\pm 1\sigma$ constraints on the cosmological parameters in Λ CDM and in the TDE scenario, as inferred from the combination of *Planck* 2018 distance prior and the M_B^{R20} prior. Noting that, $\Delta \ln \varepsilon = \ln \varepsilon_{\Lambda\text{CDM}} - \ln \varepsilon_{\text{TDE}}$.

5.1 Constraints from CMB and SH0ES

As is discussed in section 2, there is a strong degeneracy between H_0 and the late-DE parameter a_c (w) which quantify the deviation of these scenarios from Λ CDM model (see Fig. 2). Consequently, the *Planck* data alone is insufficient to give a tight constrain to these parameters, so that a prior on H_0 should be included. To test the above argument, we first consider the fit to *Planck* 2018 distance prior alone. The results tabulated in Table 2 indicates a lower bound of $a_c > 0.562$ at 68% CL, while H_0 is loosely constrained. Next, we consider the fit to a combination of *Planck* distance prior and the M_B^{R20} prior derived from SH0ES. In Table 3, we find the Hubble constant to be $H_0 = 75.2 \pm 1.7$. The H_0 tension in TDE scenario is largely removed when the M_B^{R20} prior is added. Noting that, the resolve of the tension between local distance ladder and CMB can be achieved by a wide class of “phantom-like” DE. The contours in Fig. 5 show a clear degeneracy between $a_c(\alpha)$ and H_0 in TDE model. The χ^2 statistic in 3 shows that, the goodness of the fit is significantly improved. Noted that, this improvement is mainly due to the reduction of the discordance with SH0ES data.

5.2 Constraints from Accumulative DataSets

As is discussed in previous sections, the tension between SH0ES and *Planck* is resolved by calibration of the transitional scale a_c . The problem is now transformed to, whether the expansion history (growth history) fixed by M_B^{R20} +*Planck* is in accord with other observations. If the model does restore the cosmic concordance, one would expect consistency between the fit of any dataset combinations. To verify this, we consider the constraints from accumulative datasets. We can see from Table 2, different combinations of datasets yield different values of best-fit parameters. A clear trend should be noticed that, with the inclusion of more datasets, the best-fit cosmological parameters as well as the χ^2_{\min} value approach to that of Λ CDM model. For example, with M_B^{R20} and *Planck* combination we find $H_0 = 75.2 \pm 1.7$ and $S_8 = 0.825^{+0.013}_{-0.015}$, in $\sim 3\sigma$ tension with the fit of the same datasets in Λ CDM scenario. This tension drops to less than 1σ with the inclusion of all considered likelihoods, while the differences in χ^2_{\min} value reduce from 23.5 to 3.5. With the inclusion of SNe dataset, the tension with SH0ES increased 1.9σ for TDE model. Noted that, the SNe dataset which constrains the expansion history of the late universe, i.e., $D_L(z)/H_0$, is well compatible with the Λ CDM model, thus, modification of the EoS of DE at $a \gtrsim 1/2$ is disfavored. Consequently, the $\pm 1\sigma$ constrains on transitional scale a_c decrease from 0.658 ± 0.049 to 0.548 ± 0.029 , which results in a decline of the best-fit value of H_0 . Interestingly, the tension with SH0ES reduces with the addition of a prior on $S_8 = 0.773^{+0.026}_{-0.020}$ ($S_8 = 0.833 \pm 0.016$ for the *Planck* best-fit Λ CDM). This is in accord with the shooting result shown in Fig. 2, i.e., applying such a prior on S_8 would result in a upward shift on the transitional scale a_c , which in turn increases the inferred value of H_0 . The result of Bayesian evidence analysis shows strong evidence for TDE model when LSS datasets are not considered (see last panel of Table 2). While the Bayesian evidence does not show any significant difference between TDE and Λ CDM model when all datasets are included ($\Delta \ln \varepsilon = 0.15$).

5.3 Constraints from Selected DataSets

In the context of TDE model, the tension with SH0ES increases significantly (from 1.9σ to 3.0σ) with the inclusion of BAO data. As can be seen from Fig. 4, both BAO and SNe measurements (calibrated

Dataset	Without BOSS		Without SNe	
Model	TDE	Λ CDM	TDE	Λ CDM
H_0	71.78 ± 0.90	$68.34^{+0.76}_{-0.33}$	$69.55^{+0.89}_{-1.1}$	68.17 ± 0.39
$\Omega_b h^2$	0.02250 ± 0.00013	$0.02268^{+0.00018}_{-0.00014}$	$0.02251^{+0.00016}_{-0.00013}$	$0.02266^{+0.00013}_{-0.00014}$
$\Omega_c h^2$	0.1185 ± 0.0011	$0.1169^{+0.0012}_{-0.0016}$	$0.1187^{+0.0011}_{-0.0014}$	0.11725 ± 0.00077
a_c	$0.531^{+0.045}_{-0.040}$	–	$0.419^{+0.11}_{-0.057}$	–
S_8	0.812 ± 0.012	0.7996 ± 0.0087	$0.819^{+0.011}_{-0.014}$	0.8023 ± 0.0091
$\chi^2_{M_B}$	4.8 ± 2.4	18.0 ± 4.2	11.5 ± 4.6	18.8 ± 2.4
χ^2_{Planck}	4.9 ± 3.3	11.5 ± 5.1	4.9 ± 3.8	9.1 ± 4.1
...				
χ^2_{tot}	1051.3 ± 2.8	1066.0 ± 3.9	34 ± 6	37.4 ± 2.5
$\Delta\chi^2$	–14.7	–	–3.4	–
ΔAIC	–12.5	–	–1.4	–
$\Delta \ln \varepsilon$	–4.06	–	0.23	–

Table 4. The the mean $\pm 1\sigma$ constraints on the cosmological parameters in TDE and Λ CDM models, as inferred from the combination of *Planck* 2018 distance prior; BAO data from 6dF; Pantheon SNIa data; the M_B^{R20} prior; the S_8 prior derived from DES-Y1 3x2pt data (left panel), and the *Planck* 2018 distance prior; BAO data from 6dF, SDSS DR14; M_B prior; and the S_8 prior (right panel). ΔAIC and $\Delta\chi^2$ are the differences be AIC criteria and χ^2_{min} inferred in TDE model with that of Λ CDM model, respectively. We show in the last row the pair difference of Bayesian evidence: $\Delta \ln \varepsilon = \ln \varepsilon_{\Lambda CDM} - \ln \varepsilon_{TDE}$.

Dataset	Without M_B		All combined	
Model	TDE	Λ CDM	TDE	Λ CDM
H_0	$67.82^{+0.48}_{-0.57}$	67.67 ± 0.43	69.16 ± 0.76	68.06 ± 0.41
$\Omega_b h^2$	0.02257 ± 0.00014	0.02260 ± 0.00013	0.02255 ± 0.00013	$0.02264^{+0.00013}_{-0.00011}$
$\Omega_c h^2$	0.1180 ± 0.0009	0.1181 ± 0.0009	0.1182 ± 0.0010	0.1174 ± 0.00086
a_c	< 0.252	–	$0.375^{+0.12}_{-0.043}$	–
S_8	0.818 ± 0.011	0.814 ± 0.010	0.814 ± 0.012	0.805 ± 0.010
χ^2_{Planck}	4.9 ± 3.0	5.5 ± 3.1	5.6 ± 3.5	9.9 ± 3.2
χ^2_{SN}	1034.99 ± 0.24	1034.99 ± 0.23	1068.4 ± 2.9	1034.80 ± 0.06
...				
χ^2_{tot}	1051.8 ± 2.7	1051.9 ± 2.2	1067.2 ± 2.9	1071.7 ± 2.2
$\Delta\chi^2$	–0.1	–	–4.5	–
ΔAIC	1.9	–	–2.5	–
$\Delta \ln \varepsilon$	2.74	–	0.15	–

Table 5. The the mean $\pm 1\sigma$ constraints on the cosmological parameters in TDE and Λ CDM models, as inferred from the combination of *Planck* 2018 distance prior; BAO data from 6dF, SDSS DR14, and BOSS DR12; Pantheon SNIa data; BOSS DR12 RSD data; and the S_8 prior derived from DES-Y1 3x2pt data (left panel), and *Planck* 2018 distance prior; BAO data from 6dF, SDSS DR14; M_B ; SNe dataset and the S_8 prior (right panel). ΔAIC and $\Delta\chi^2$ are the differences between the value of AIC criteria and χ^2_{min} inferred in TDE model with that of Λ CDM model, respectively. The pair difference of Bayesian evidence given in the last row is: $\Delta \ln \varepsilon = \ln \varepsilon_{\Lambda CDM} - \ln \varepsilon_{TDE}$.

by the local distance ladder) anchor the distance scale at $z \lesssim 1.0$, yet not in good agreement with each other. Such tension is inherited in the dataset itself. Therefore, the conformity with one of the anchor almost certainly leads to discordance with the other. While within the scenarios of late-DE, the inferred r_s is identical with fiducial Λ CDM model (see section 2), so the discordance between BAO and SNe (H_0) datasets can't be reconciled. However, the BAO mea-

surements rely on the presumption of the fiducial cosmology, which means the measured distance scale should be calibrated by the factor $r_{d, fid}/r_d$. To account for the possibility that the tension is originated by some unknown systematics of a single dataset, we selected several subclasses of whole datasets as follows:

- Without BOSS: Comparing the result tabulated in Table 4 and

Table 5, we find that with the exclusion of BOSS dataset, the $\pm 1\sigma$ constrains on H_0 increase from 69.16 ± 0.76 to 71.77 ± 0.90 while the tension with SH0ES reduce from 3.2σ to 1.9σ (see Fig. 6 for a view) in TDE model. Which indicates that the tension between BOSS and M_B^{R20} prior derived from SH0ES can not be reconciled in this scenario.

- Without SNe: See Table 4 and Table 5 for a contrast between the constraint results with and without SNe dataset. As can be seen, the best-fit transitional scale a_c as well as other cosmological parameters (including H_0) are almost identical in both case, suggesting that the SNe dataset is well compatible with the TDE scenario.

- Without M_B^{R20} : From Table 5 one can see that, the difference in $\pm 1\sigma$ constrains on H_0 for the two model is marginal, also are the χ^2 statistics, i.e., $\Delta\chi^2 = -0.1$. In this case, the extra late-DE parameter is redundant. The numerical results suggest that, the transitional scale a_c is consistent with zero, i.e., $a_c < 0.252$. Meanwhile, the Bayesian evidence is against the TDE model when compared with the fiducial Λ CDM model ($\Delta \ln \mathcal{E} = 2.74$).

For a brief summary, the TDE scenario is disfavored by the BAO dataset. This discordance could not be fully removed within the context of late-DE. With the exclusion of M_B^{R20} prior and the inclusion of LSS dataset, the Λ CDM model is favored over TDE model.

6 DISCUSSION AND CONCLUSIONS

The Λ CDM model calibrated by *Planck* data is well compatible with a large bunch of independent observational datasets (BAO, SN Ia, etc), but in severe tension with the local distance ladder (H_0). Consequently, the ideal solution to the discordance lies in the scenarios which disagree with Λ CDM solely on the inferences of H_0 , while recover the predictions of Λ CDM in most cases. However, the shift in H_0 inevitably leads to the modification in late expansion history. A practical way to capture this modification is to add an extra parameter to the six standard Λ CDM parameters named as “late-DE parameter”, which degenerates only with H_0 while is uncorrelated with the other five parameters.

In this work, we explore a representative parameterization within the scenarios of late dark energy: a novel version of Transitional dark energy (TDE). The main feature of the TDE model is the sharp transition of the EoS of DE at the critical scale a_c . When a_c approach to zero, the TDE model recovers Λ CDM model. We analyze the TDE scenario accounting for *Planck* 2018 distance prior, BAO+FS (DF6, BOSS DR12 and DR14), S_8 prior derived from DES-Y1 3x2pt, as well as the M_B^{R20} prior derived from SH0ES and SNe dataset from the Pantheon compilation. The results are shown in Table 3–5 and Fig. 5–7. To give a clear view on the influences of different datasets, we conduct the MCMC analysis in an accumulative way. Due to the degeneracy between H_0 and the extra late-DE parameter, H_0 is loosely constrained by CMB alone, i.e., $H_0 = 77.0 \pm 8.0$ for TDE model. When added with the M_B^{R20} prior, the constraint results for TDE ($H_0 = 75.2 \pm 1.7$) closely match the SH0ES H_0 prior, which further confirms the degeneracy. With the growing number of included datasets, one can see clear trend that the TDE scenario degenerates into standard Λ CDM model, meanwhile, the tension with SH0ES grows continuously (see Table 2). Thus, the tension on H_0 is not solved, also, the S_8 tension is neither relieved nor exacerbated in TDE scenario. Owing to the fact that the structure growth is more rapid in the case of “phantom-like” DE than that of cosmological constant, a lower inferred value of $\Omega_{m,0}$ is largely compensated by

the upward shift on σ_8 , resulting in a minor influence on the S_8 constraints.

The three main anchors of the cosmic distance scale, e.g., CMB ($z \sim 1100$), BAO ($z \sim 0.3$), and SNe Ia calibrated by the local H_0 measurements ($z \lesssim 1.5$) form a “Impossible trinity”, i.e., it’s plausible to reconcile with any two of the three but hard to accommodate all of them. Within the scenarios of late-DE, it’s nearly impossible to reconcile the tension between BAO ($z \sim 0.3$) and SNe Ia calibrated by H_0 (see Fig. 4). Even if we allow for a reduction of the sound horizon r_s , it is not likely to simultaneously match the distance anchored by CMB and BAO (see D’Amico et al. (2020); Hill et al. (2020)), because given a certain shift in r_s , the shift in H_0 needed to match the CMB observations will be different than the one needed to match the late LSS observations. However, the late universe measurements require the modeling of complex astrophysical systems which may bring about some systematic error either in the measurements or in the astrophysical modeling (D’Amico et al. (2020); Mortsell et al. (2021)). To account for the possibility of unknown systematics, we selected several subclasses of the datasets, the constraint results can be seen in Table 4, 5 and Fig. 6. In the analysis without BOSS measurement, TDE model have shown its potential to solve the H_0 tension, i.e., $H_0 = 71.77 \pm 0.90$ and $a_c = 0.531^{+0.045}_{-0.040}$ (reconcile with SH0ES within 2σ). This result can also be verified by “shooting”, which suggests that, at $a_c = 0.531$ the *Planck* best-fit value is $H_0 = 72.19$ (see Fig. 2). With the combination of all considered datasets (including M_B^{R20}), we see a positive sign that the EoS transits in TDE scenario, i.e., the transitional scale of DE is not consistent with zero ($a_c = 0.375^{+0.12}_{-0.043}$ at 68% CL). With the exclusion of the M_B^{R20} prior, we have a_c peaked toward zero. In this case, the result of Bayesian evidence analysis is against TDE model when compared with Λ CDM model. However, the analysis without BOSS measurement indicates strong evidence for TDE model ($\Delta \ln \mathcal{E} = 4.06$).

In summary, owing to the irreconcilable tension between BAO and SNe Ia calibrated by H_0 , within the scenario of TDE the cosmological concordance can not be restored. However, with the presumption of unknown systematics, the TDE model could still be viewed as a viable candidate. What is the “true” origin of these discordances? We hope that more investigators will be motivated to explore this sector.

ACKNOWLEDGEMENTS

This work is supported in part by National Natural Science Foundation of China under Grant No.12075042, Grant No.11675032 (People’s Republic of China).

DATA AVAILABILITY

The data underlying this article will be shared on reasonable request to the corresponding author.

REFERENCES

- Abbott T., et al., 2018, *Phys. Rev. D*, 98, 043526
- Ade P., et al., 2014, *Astron. Astrophys.*, 571, A16
- Aghanim N., et al., 2018
- Aghanim N., et al., 2020, *Astron. Astrophys.*, 641, A5
- Akaike H., 1974, *IEEE Transactions of Automatic Control*, 19, 716
- Alam S., et al., 2017, *Mon. Not. Roy. Astron. Soc.*, 470, 2617

- Aleasant G., Perivolaropoulos L., 2021, *Mon. Not. Roy. Astron. Soc.*, 504, 3956
- Aleasant G., Kazantzidis L., Perivolaropoulos L., 2020, *Phys. Rev. D*, 101, 123516
- Aleasant G., Antoniou I., Perivolaropoulos L., 2021a, *Universe*, 7, 366
- Aleasant G., Kazantzidis L., Perivolaropoulos L., 2021b, *Phys. Rev. D*, 103, 083517
- Armendariz-Picon C., Mukhanov V. F., Steinhardt P. J., 2000, *Phys. Rev. Lett.*, 85, 4438
- Armendariz-Picon C., Mukhanov V. F., Steinhardt P. J., 2001, *Phys. Rev.*, D63, 103510
- Ballardini M., Braglia M., Finelli F., Paoletti D., Starobinsky A. A., Umiltà C., 2020, *JCAP*, 10, 044
- Ballesteros G., Lesgourgues J., 2010, *JCAP*, 10, 014
- Banerjee A., Cai H., Heisenberg L., Colgáin E. O., Sheikh-Jabbari M. M., Yang T., 2021, *Phys. Rev. D*, 103, L081305
- Barboza Jr. E. M., Alcaniz J. S., 2008, *Phys. Lett.*, B666, 415
- Bassett B. A., Kunz M., Silk J., Ungarelli C., 2002, *Mon. Not. Roy. Astron. Soc.*, 336, 1217
- Bautista J. E., et al., 2017, *Astron. Astrophys.*, 603, A12
- Benaoum H. B., Yang W., Pan S., Di Valentino E., 2020
- Benevento G., Hu W., Raveri M., 2020, *Phys. Rev. D*, 101, 103517
- Beutler F., et al., 2011, *Mon. Not. Roy. Astron. Soc.*, 416, 3017
- Blas D., Lesgourgues J., Tram T., 2011, *JCAP*, 07, 034
- Caldwell R. R., 2002, *Phys. Lett.*, B545, 23
- Caldwell R. R., Kamionkowski M., Weinberg N. N., 2003, *Phys. Rev. Lett.*, 91, 071301
- Camarena D., Marra V., 2020a, *Phys. Rev. Res.*, 2, 013028
- Camarena D., Marra V., 2020b, *Mon. Not. Roy. Astron. Soc.*, 495, 2630
- Camarena D., Marra V., 2021, *JCAP*, 10.1093/mnras/stab1200
- Chen L., Huang Q.-G., Wang K., 2019, *JCAP*, 02, 028
- Chiang C.-T., Slosar A., 2018
- D'Agostino R., Nunes R. C., 2020, *Phys. Rev. D*, 101, 103505
- D'Amico G., Senatore L., Zhang P., Zheng H., 2020
- D'Amico G., Senatore L., Zhang P., 2021, *JCAP*, 01, 006
- Dainotti M. G., De Simone B., Schiavone T., Montani G., Rinaldi E., Lambiase G., 2021, *Astrophys. J.*, 912, 150
- De Felice A., Tsujikawa S., 2010, *Phys. Rev. Lett.*, 105, 111301
- Di Valentino E., Melchiorri A., Mena O., Vagnozzi S., 2020, *Phys. Dark Univ.*, 30, 100666
- Di Valentino E., et al., 2021
- Efstathiou G., 2021, *Mon. Not. Roy. Astron. Soc.*, 505, 3866
- Freedman W. L., 2021
- Frusciante N., Peirone S., Atayde L., De Felice A., 2020, *Phys. Rev. D*, 101, 064001
- Gelman A., Rubin D. B., 1992, *Statistical Science*, 7, 457
- Gil-Marín H., et al., 2018, *Mon. Not. Roy. Astron. Soc.*, 477, 1604
- Gogoi A., Sharma R. K., Chanda P., Das S., 2020
- Guo Z.-K., Piao Y.-S., Zhang X.-M., Zhang Y.-Z., 2005, *Phys. Lett.*, B608, 177
- Hart L., Chluba J., 2018, *Mon. Not. Roy. Astron. Soc.*, 474, 1850
- Hernández-Almada A., Leon G., Magaña J., García-Aspeitia M. A., Motta V., 2020, *Mon. Not. Roy. Astron. Soc.*, 497, 1590
- Hikage C., et al., 2019, *Publ. Astron. Soc. Jap.*, 71, Publications of the Astronomical Society of Japan, Volume 71, Issue 2, April 2019, 43, <https://doi.org/10.1093/pasj/psz010>
- Hildebrandt H., et al., 2020, *Astron. Astrophys.*, 633, A69
- Hill J. C., McDonough E., Toomey M. W., Alexander S., 2020, *Phys. Rev. D*, 102, 043507
- Hinshaw G., et al., 2013, *The Astrophysical Journal Supplement Series*, 208, 19
- Jassal H. K., Bagla J. S., Padmanabhan T., 2005, *Mon. Not. Roy. Astron. Soc.*, 356, L11
- Jedamzik K., Pogosian L., 2020, *Phys. Rev. Lett.*, 125, 181302
- Jeffreys H., 1961, *Theory of Probability*
- Kazantzidis L., Perivolaropoulos L., 2018, *Phys. Rev. D*, 97, 103503
- Keeley R. E., Joudaki S., Kaplinghat M., Kirkby D., 2019, *JCAP*, 12, 035
- Knox L., Millea M., 2020, *Phys. Rev. D*, 101, 043533
- Kumar S., Nunes R. C., 2016, *Phys. Rev. D*, 94, 123511
- Lesgourgues J., 2011
- Lewis A., 2019
- Li X., Shafieloo A., 2019, *Astrophys. J. Lett.*, 883, L3
- Li X., Shafieloo A., 2020, *Astrophys. J.*, 902, 58
- Li M., Li X.-D., Wang S., Wang Y., 2011, *Communications in Theoretical Physics*, 56, 525
- Li E.-K., Du M., Zhou Z.-H., Zhang H., Xu L., 2021, *Mon. Not. Roy. Astron. Soc.*, 501, 4452
- Lin M.-X., Hu W., Raveri M., 2020, *Phys. Rev. D*, 102, 123523
- Linder E. V., 2003, *Phys. Rev. Lett.*, 90, 091301
- Lonappan A. I., Kumar S., Ruchika Dinda B. R., Sen A. A., 2018, *Phys. Rev. D*, 97, 043524
- Marra V., Perivolaropoulos L., 2021, *Phys. Rev. D*, 104, L021303
- Mead A., 2017, *Mon. Not. Roy. Astron. Soc.*, 464, 1282
- Mead A., Peacock J., Heymans C., Joudaki S., Heavens A., 2015, *Mon. Not. Roy. Astron. Soc.*, 454, 1958
- Mead A., Brieden S., Tröster T., Heymans C., 2020, *JCAP*, 10.1093/mnras/stab082
- Mehrabi A., Basilakos S., 2018, *Eur. Phys. J.*, C78, 889
- Mortsell E., Goobar A., Johansson J., Dhawan S., 2021
- Nunes R. C., 2018, *JCAP*, 05, 052
- Nunes R. C., Di Valentino E., 2021, *Phys. Rev. D*, 104, 063529
- Pan S., Sharov G. S., Yang W., 2020, *Phys. Rev. D*, 101, 103533
- Perivolaropoulos L., Skara F., 2021a
- Perivolaropoulos L., Skara F., 2021b
- Poulin V., Smith T. L., Grin D., Karwal T., Kamionkowski M., 2018, *Phys. Rev. D*, 98, 083525
- Poulin V., Smith T. L., Karwal T., Kamionkowski M., 2019, *Phys. Rev. Lett.*, 122, 221301
- Raveri M., 2020, *Phys. Rev. D*, 101, 083524
- Rezaei M., Naderi T., Malekjani M., Mehrabi A., 2020, *Eur. Phys. J. C*, 80, 374
- Riess A. G., Casertano S., Yuan W., Bowers J. B., Macri L., Zinn J. C., Scolnic D., 2021, *Astrophys. J. Lett.*, 908, L6
- Saini T. D., Weller J., Bridle S. L., 2004, *Mon. Not. Roy. Astron. Soc.*, 348, 603
- Sandage A., Tammann G., Saha A., Reindl B., Macchetto F., Panagia N., 2006, *Astrophys. J.*, 653, 843
- Saridakis E. N., et al., 2021
- Scolnic D. M., et al., 2018, *Astrophys. J.*, 859, 101
- Sekiguchi T., Takahashi T., 2020
- Shafieloo A., Sahni V., Starobinsky A. A., 2009, *Phys. Rev. D*, 80, 101301
- Torrado J., Lewis A., 2020
- Vagnozzi S., 2020, *Phys. Rev. D*, 102, 023518
- Verde L., Treu T., Riess A., 2019, *Nature Astron.*, 3, 891
- Visinelli L., Vagnozzi S., Danielsson U., 2019, *Symmetry*, 11, 1035
- Wong K. C., et al., 2020, *Mon. Not. Roy. Astron. Soc.*, 498, 1420
- Yan S.-F., Zhang P., Chen J.-W., Zhang X.-Z., Cai Y.-F., Saridakis E. N., 2020, *Phys. Rev. D*, 101, 121301
- Yang W., Pan S., Di Valentino E., Nunes R. C., Vagnozzi S., Mota D. F., 2018, *JCAP*, 09, 019
- Yang W., Pan S., Paliathanasis A., Ghosh S., Wu Y., 2019, *Mon. Not. Roy. Astron. Soc.*, 490, 2071

APPENDIX A: PRIOR DEPENDENCE

We have assumed uniform prior probability distributions for effective TDE parameter a_c , which correspond to non-uniform priors on the transitional redshifts $z_c = 1/a_c - 1$. The EoS in parameterized by z_c (denote as TDE(z_c)) can be rewritten as:

$$w(z) = -1 - \frac{1}{2} [\tanh(3(z - z_c)) + 1] \quad (\text{A1})$$

An obvious concern is the dependence of the posterior distributions on the choice of priors. To account for that, we recompute the TDE parameter constraints with a uniform prior imposed on z_c , i.e.,

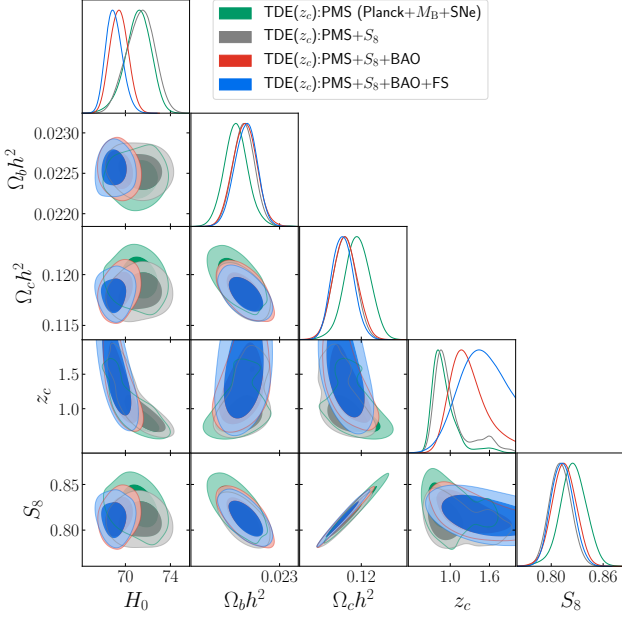


Figure A1. Constraints on TDE scenario with a uniform prior on z_c (denote as TDE(z_c)) from various dataset combinations. The contours show 1σ and 2σ posteriors. The constraints on cosmological parameters closely match the results shown in the left panel of Fig. 7.

$z_c \in [0, 100]$, which corresponds to $a_c \in [0.01, 1]$. The posterior distributions are shown in Fig. A1 and the parameter constraints are tabulated in Table A1. It's obvious to see that, the difference in priors have a negligible impact on the χ^2 statistics, e.g., $\chi^2_{min} = 1068.4$ for the TDE fit to the all combined datasets and $\chi^2_{min} = 1068.7$ for that of TDE(z_c) fit of all combined datasets. It is notable that, there is a slight decline on the inferred value of H_0 in TDE(z_c), which could be understood as the effect of a shift in prior probability distribution toward a smaller value of a_c when a uniform prior on z_c is assumed. The difference between the fit of TDE and TDE(z_c) becomes insignificant with the inclusion of a growing number of datasets (see Table A1).

APPENDIX B: TWO PARAMETERS TDE(2P)

In previous sections we have fixed $w_0 = -1$ to recover Λ CDM when $a \gtrsim a_c$. While in this section, w_0 is considered as a free constant. In this case, the transitional DE is described by two parameters (w_0, a_c). The parameter constraints and the posterior distributions are shown in Table A1 and Fig. B1. From the middle panel of Table A1 one can see that, the constraints in TDE(2p) model on $\Omega_b h^2, \Omega_c h^2$ and S_8 from each dataset combination closely match that of TDE(1p) model, while the constraint on w_0 is in agreement with -1 within 2σ . As can be noticed, there is a slight downward shift on the fit of w_0 from $w_0 \gtrsim -1$ to $w_0 \lesssim -1$ with the inclusion of BAO datasets. As is discussed in section 3, the downward shift on w_0 would increase the dilution rate of DE, which lowers inferred value of θ_{LSS} while increases the growth function $f(z)$ in the late universe. As to χ^2 statistics, adding a free parameter (w_0) has negligible improvement on the goodness of the fit (see the third panel of Table A1). So effectively speaking, the TDE model is efficiently captured by a single parameter a_c . As is shown in the last column of Table A1, we have compared the Bayesian evidence between TDE and TDE(2p) model. In the case of all datasets combination, we find $\Delta\mathcal{E} = 0.26$ indicating the weak evidence against TDE(2p).

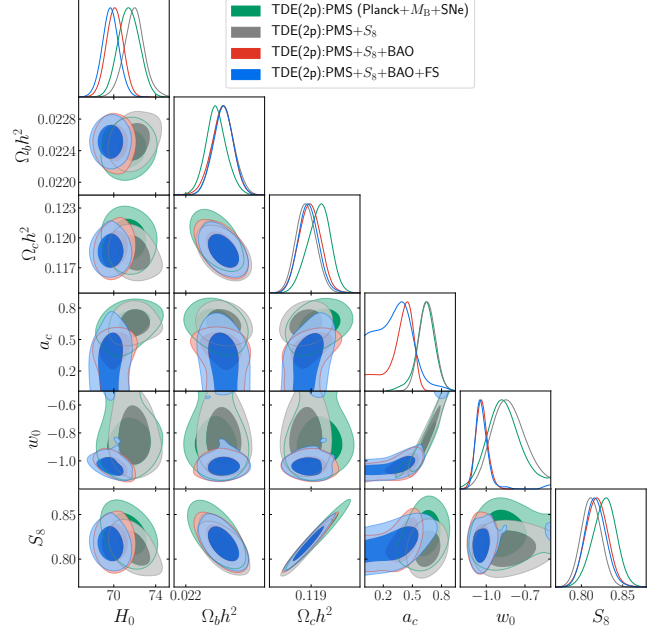


Figure B1. Constraints on two parameters TDE(2p) model from various dataset combinations. The contours show 1σ and 2σ posteriors. See Table A1 for the mean $\pm 1\sigma$ constraints on the cosmological parameters.

APPENDIX C: PLANCK TTTEEE RESULTS

The constraint results from the *Planck* 2018 low- ℓ TT+EE and *Planck* 2018 high- ℓ TT+TE+EE temperature and polarization power spectrum and several dataset combinations are tabulated in the last panel of Table A1, and the posterior distributions are shown in Fig. C1. Note that, the constraints on H_0, a_c and S_8 from *Planck* TT+TE+EE data closely matches the results obtained from the *Planck* distance prior.

This paper has been typeset from a \LaTeX file prepared by the author.

Model	Dataset	H_0	S_8	a_c		$\ln \varepsilon$	$\Delta \ln \varepsilon$	χ^2_{\min}
TDE	<i>Planck</i> + M_B	75.2 ± 1.7	$0.825^{+0.013}_{-0.015}$	0.658 ± 0.049	–	-11.54	–	4.6
	PMS	71.59 ± 0.81	0.825 ± 0.011	0.548 ± 0.029	–	-533.04	–	1045.0
	PMS+ S_8	71.77 ± 0.90	0.812 ± 0.012	$0.531^{+0.045}_{-0.040}$	–	-535.07	–	1051.3
	PMS+ S_8 +BAO	$69.55^{+0.73}_{-0.94}$	0.816 ± 0.015	0.420 ± 0.082	–	-540.25	–	1062.3
	PMS+ S_8 +BAO +FS	69.16 ± 0.76	0.814 ± 0.012	$0.375^{+0.12}_{-0.043}$	–	-543.41	–	1068.4
		H_0	S_8	a_c	w_0	$\ln \varepsilon$	$\Delta \ln \varepsilon$	χ^2_{\min}
TDE(2p)	<i>Planck</i> + M_B	74.6 ± 1.5	0.824 ± 0.014	$0.50^{+0.027}_{-0.033}$	> -1.23	-7.52	-4.02	4.1
	PMS	71.44 ± 0.93	0.828 ± 0.013	$0.638^{+0.078}_{-0.062}$	$-0.86^{+0.12}_{-0.14}$	-532.95	-0.09	1045.3
	PMS+ S_8	70.09 ± 0.78	0.812 ± 0.012	0.652 ± 0.078	$-0.83^{+0.12}_{-0.14}$	-535.17	0.10	1049.5
	PMS+ S_8 +BAO	70.25 ± 0.79	0.819 ± 0.013	$0.378^{+0.16}_{-0.064}$	$-1.04^{+0.04}_{-0.05}$	-539.71	-0.54	1061.7
	PMS+ S_8 +BAO+FS	69.69 ± 0.79	0.817 ± 0.012	$0.32^{+0.17}_{-0.20}$	$-1.02^{+0.02}_{-0.07}$	-543.67	0.26	1069.0
		H_0	S_8	z_c				χ^2_{\min}
TDE(z_c)	<i>Planck</i> + M_B	73.8 ± 2.1	0.825 ± 0.014	0.63 ± 0.15	–	–	–	–
	PMS	$71.1^{+1.2}_{-1.0}$	$0.825^{+0.015}_{-0.018}$	$0.91^{+0.08}_{-0.19}$	–	–	–	1046.8
	PMS+ S_8	$71.3^{+1.3}_{-1.2}$	0.811 ± 0.012	$1.014^{+0.062}_{-0.30}$	–	–	–	1051.1
	PMS+ S_8 +BAO	69.43 ± 0.78	0.815 ± 0.014	$1.643^{+0.048}_{-0.79}$	–	–	–	1061.8
	PMS+ S_8 +BAO +FS	$69.0^{+0.66}_{-0.81}$	0.813 ± 0.013	$1.88^{+0.38}_{-0.92}$	–	–	–	1068.7
		H_0	S_8	a_c	τ_{reio}	$\log(10^{10} A_s)$	n_s	χ^2_{\min}
TDE	<i>Planck</i> :TTTEEE + M_B	74.8 ± 1.9	$0.812^{+0.018}_{-0.015}$	$0.613^{+0.054}_{-0.047}$	$0.0527^{+0.0087}_{-0.0074}$	$3.039^{+0.020}_{-0.014}$	$0.9665^{+0.0042}_{-0.0060}$	1012
	TMS	72.0 ± 1.2	0.818 ± 0.017	$0.535^{+0.042}_{-0.034}$	$0.0522^{+0.0085}_{-0.0086}$	$3.039^{+0.017}_{-0.018}$	$0.9660^{+0.0041}_{-0.0043}$	2050
	TMS+ S_8	$71.9^{+1.2}_{-0.90}$	0.807 ± 0.014	$0.517^{+0.041}_{-0.032}$	$0.0516^{+0.0088}_{-0.0077}$	$3.035^{+0.020}_{-0.014}$	$0.9673^{+0.0054}_{-0.0037}$	2057
	TMS+ S_8 +BAO	$69.84^{+0.64}_{-0.84}$	$0.812^{+0.015}_{-0.011}$	$0.398^{+0.10}_{-0.031}$	$0.0536^{+0.0075}_{-0.0096}$	$3.039^{+0.017}_{-0.018}$	$0.9685^{+0.0042}_{-0.0054}$	2068
	TMS+ S_8 +BAO +FS	$69.29^{+0.67}_{-0.77}$	0.811 ± 0.013	$0.351^{+0.12}_{-0.045}$	$0.0530^{+0.0072}_{-0.0094}$	$3.037^{+0.015}_{-0.019}$	$0.9682^{+0.0045}_{-0.0047}$	2072

Table A1. The the mean $\pm 1\sigma$ constraints on the cosmological parameters in TDE model parameterized by a_c (first panel), TDE(2p) parameterized by a_c and w_0 (second panel), TDE model parameterized by z_c (third panel), and TDE model constrained by *Planck* TT+TE+EE data and several dataset combinations (fourth panel). Noted that the pair difference of Bayesian evidence is given by: $\Delta \ln \varepsilon = \ln \varepsilon_{\text{TDE}} - \ln \varepsilon_{\text{TDE}(2p)}$.

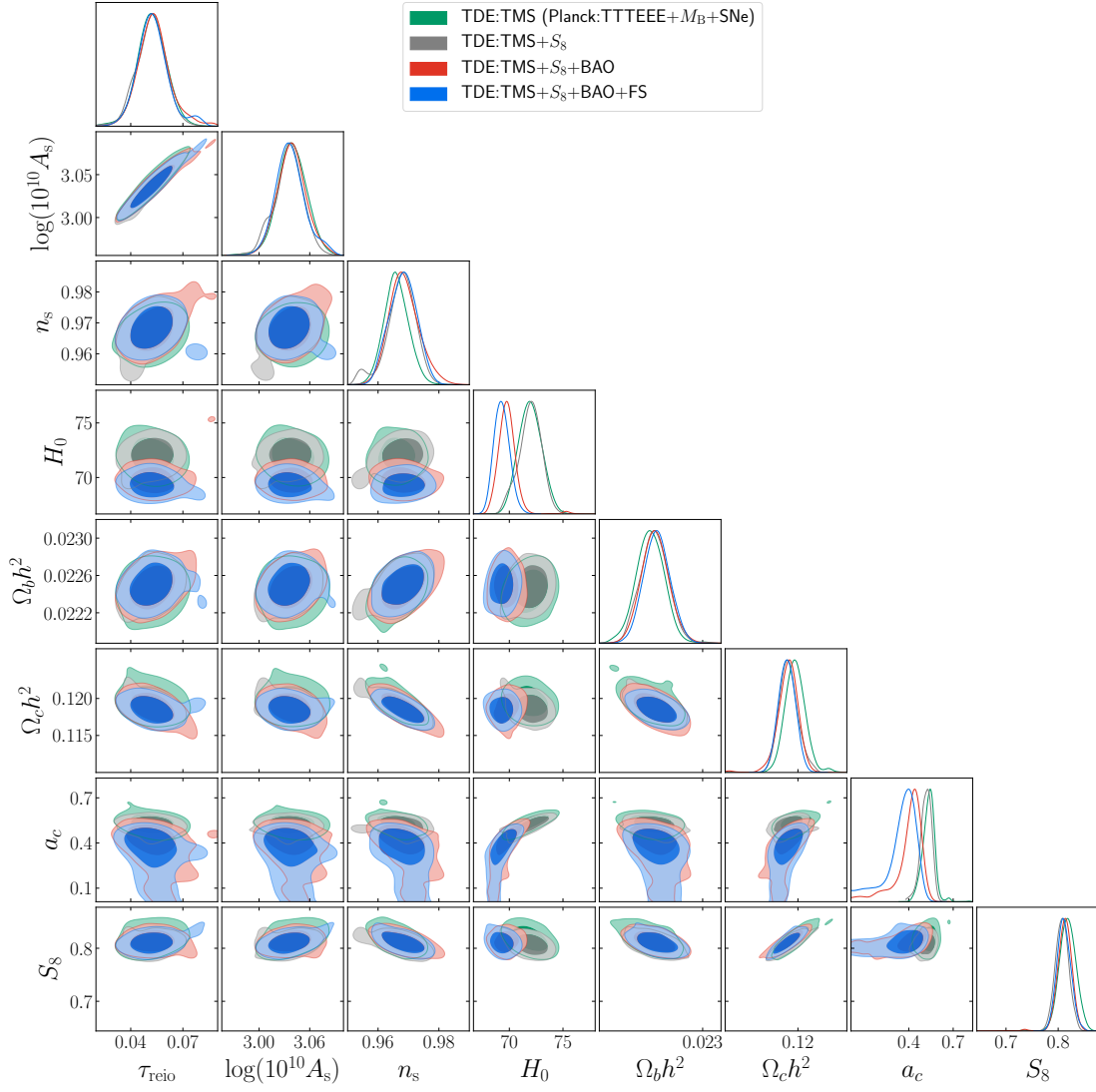


Figure C1. Constraints on TDE scenario with *Planck* TT+TE+EE data and several dataset combinations. The contours show 1σ and 2σ posteriors.